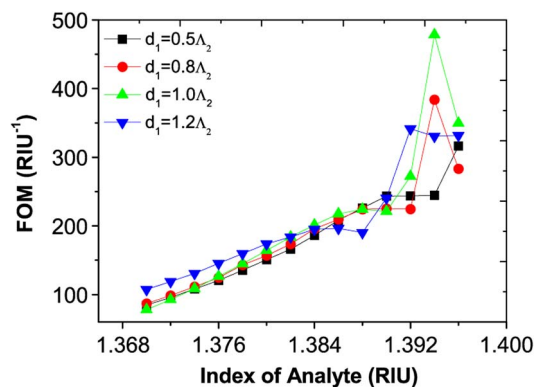# A Surface Plasmon Biosensor Based on a D-Shaped Microstructured Optical Fiber With Rectangular Lattice

Lu Peng
Fukun Shi
Guiyao Zhou
Shu Ge
Zhiyun Hou
Changming Xia

A Surface Plasmon Biosensor Based on a D-Shaped Microstructured Optical Fiber With Rectangular Lattice

Lu Peng, Fukun Shi, Guiyao Zhou, Shu Ge, Zhiyun Hou, and Changming Xia

[1]Guangdong Province Key Laboratory of Nanophotonic Functional Materials and Devices, South China Normal University, Guangzhou 510006, China
[2]Specially Functional Fiber Engineering Technology Research Center of Guangdong Higher Education Institutes, South China Normal University, Guangzhou 510006, China

Abstract: A numerical investigation of a surface plasmon biosensor based on D-shaped microstructured optical fiber (MOF) with rectangular lattice is presented. A full-vector finite-element method is applied to analyze the resonance coupling properties. By adjusting the diameters of two large air holes, the proposed biosensor shows excellent performance. High sensitivity and narrow full-width at half-maximum (FWHM) can be achieved. In particular, the figure of merit can reach to 478.3RIU^{-1}, which is to our knowledge the highest among the reported MOF sensors. In the last part, the influence of coating thickness on the sensing performance has been considered.

Index Terms: Surface plasmon, fiber optics sensors, microstructured optical fibers.

1. Introduction

The surface plasmon resonance (SPR)-based sensing technique has attracted much attention in recent years owing to its effective and precision in sensing method [1], [2]. Intensive photon-electron interaction in the interface of metal and dielectric forms surface plasmon polaritons (SPPs), and the resonance occurs when the core guided mode is coupled to the plasmon modes [3]. A slight variation of the environmental refractive index has a deep effect on the resonance coupling, it shows an enormous potential application both in biological and chemical sensor [4]–[6]. SPR sensor based on microstructure fibers has high sensitivity and compact configuration, which is stepped into extensive applications such as the food safety, medicine testing, and environment monitoring [7]–[9].

Microstructured optical fibers (MOFs), also known as photonic crystal fibers (PCFs) or holey fibers (HFs), is composed of many tiny air holes along the fiber length based on silica glass. Its flexible structure can extend some new characteristics through filling the cladding air holes with materials such as semiconductor [10], liquid crystal [11], or metal [12], [13]. The combination of MOFs and metal opens up a stage for high performance sensing. However, the fabrication of depositing metal film or wires into the air holes of MOFs is not an easy thing. Then, D-shaped

fiber was proposed which one side of the fiber was polished, and a thin film of metal was deposited on the polishing surface to excite SPR. The designation of D-shaped fiber makes the coating film on the outside of a fiber easier to manufacture [14], [15].

According to [16], a D-shaped rectangular lattice microstructured optical fiber offered two larger leaky channels, which can significantly enhance the resonance between the plasmon waves and core guided wave. Higher sensitivity was achieved in reference [16], however, the multiple resonance peaks and large spectral width would deteriorate the signal-to-noise ratio (SNR) that is not desirable in the practical sensing applications. It is no doubt that sharper peaks will result in large FOM. Various investigations concerning high-performance plasmonic or MOFs sensor have been reported over the past years [17]–[19]. Yanik *et al.* [20] experimentally demonstrated an ultrasensitive label-free detective technique based on asymmetric Fano resonances with FOM 162. Gao *et al.* [5] experimentally proposed a plasmonic interferometric biosensor with FOM 146. Shen *et al.* [21] experimentally showed a plasmonic gold mushroom arrays with refractive sensing and the FOM reached to 108. We can find that the record-high FOM in the experiment is 162 for plasmonic sensing. Also, some theoretical investigations are reported specific to the field of MOFs sensors. Tian *et al.* [22] presented a all solid D-shaped PCF sensor via numerical simulation with the high FOM 216. Fan *et al.* [23] reported an analyte-filled photonic crystal fiber (AF-PCF) sensor based on surface plasmon resonance and the discussed FOM near 170 by theoretical simulation.

In this paper, we present a D-shaped MOF biosensor with rectangular lattice introduced two large air holes which helps to keep the parallel between the polished side and the first upper row of air holes in the fabrication process as in our previous designation [24]. Though numerically investigating the coupling properties for different holes size, we found that the sensing performance is deeply affected by two large leaky channels and birefringence. Simulated results indicated that high sensitivity 7481 nm/RIU and narrow full-width at half-maximum (FWHM) 13.6 nm are acquired in proposed sensor. Furthermore, the FOM is up to 478.3 which is higher than previous reports [22], [23]. Narrower spectral width and high FOM presented in our paper reveal excellent sensing performance in terms of filtering the noise and better detection limit.

2. Model Designed

A three-dimensional schematic is shown in Fig. 1. The background material, blue area in the Fig. 1, is composed of pure silica glass and air holes (black) arrangement with rectangular lattice. The core of the MOF is shaped by moving a center air hole and replacing it with pure silica glass. The bottom portion of MOF is polished and a thin film of gold (golden) is deposited on the bottom flat surface. As we can see from the Fig. 1, the horizontal lattice pitch is $\Lambda_1 = 2$ μm and the vertical lattice pitch is $\Lambda_2 = 1.5$ μm, respectively. The thickness of the gold film is $th = 40$ nm, and where it touches the analyte liquids. In this paper, we use n_a to represent the refractive index (RI) of analyte. The two air holes next to the core have larger diameters, which result in the different birefringence. All remaining air holes keep the same diameter $d_2 = 0.75$ μm under all conditions. The finite element method (FEM) with perfectly matched layers (PMLs) has been applied to investigate the guiding and coupling properties [3]. Surface plasmon waves excited because of the penetrative energy from the core guided wave. When the phase of the surface plasmonic modes and the core mode matched, the resonance occurs.

The dielectric function of gold is described by the modified Drude–Lorentz model [25]. In the same time, the material dispersion of silica glass is accounted by Sellmeier equation [26]. The confinement loss can be expressed as

$$\frac{20}{\ln(10)} \times \frac{2\pi}{\lambda} \times \text{Im}(n_{\text{eff}}) \quad \text{(in dB per unit length)} \tag{1}$$

where λ represents the vacuum wavelength, and $\text{Im}(n_{\text{eff}})$ is the imaginary part of the effective index.
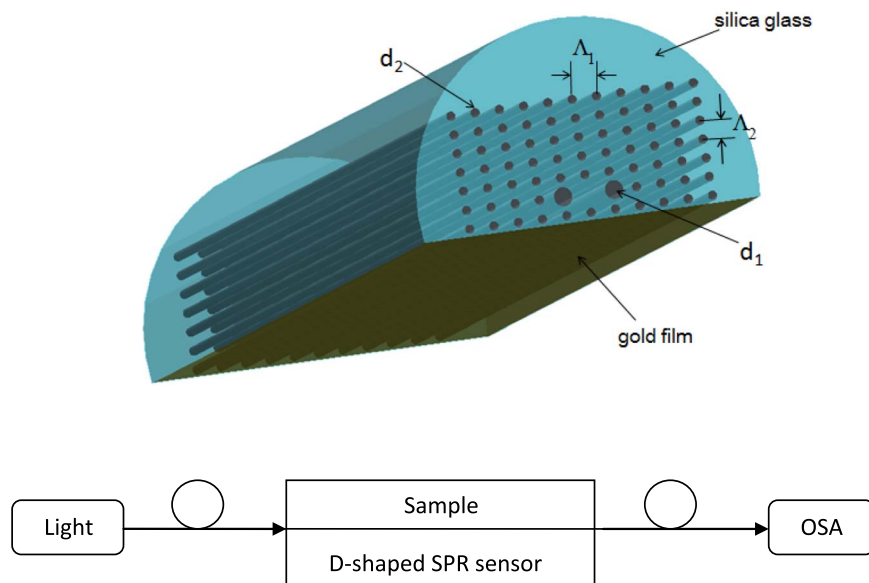
Fig. 1. Three dimensional schematic of the D-shaped microstructure fiber with rectangular lattice and the corresponding experimental setup.

3. Simulated Results and Analysis

3.1. The Coupling Properties

At first, we investigated the coupling properties of MOF by changing the diameter of the two air holes around the fiber core as shown in Fig. 1. The left patterns in Fig. 2 plot the resonance properties between the core mode and surface plasmon modes with different diameter of d_1. The upper part gives the case at the analyte RI of 1.38, the lower one is 1.386. The resonance occurs at the crossing point where the dispersion lines of the core mode and the plasmonic mode coincide. In Fig. 2(a) and (c), the black lines represent the dispersive curve of second-order plasmonic mode. The two graphs on the right of Fig. 2 show the core fundamental mode's spatial distribution of electric field density at the resonance wavelength for different hole sizes of d_1 with the analyte RI of 1.38 (upper) and 1.386 (lower), respectively.

In Fig. 2(a), the loss peaks appear in the s-shaped kinks where the core mode and plasmonic second-order mode (black) interact, it supposes that only second-order plasmonic mode can couple to the guided core fundamental mode in circumstance of this analyte RI. Noticing that the values of different loss peaks for $d_1 = 0.5\Lambda_2$, $0.8\Lambda_2$, and $1.0\Lambda_2$ are almost equal, however, the loss peak of $d_1 = 1.2\Lambda_2$ is significantly lower. Accordingly, the tendency repeats in the Fig. 2(b), the corresponding electric field distributions provide intuitional degrees to understand the tendency. With the increase of d_1, the electric field intensity of core mode raises slightly as well, which means there is less energy leaking to surface plasmon modes from fiber core, that is simply because of the suppression of the leaky channel and the diminution of effective mode area both result from the bigger air holes. The difference of loss peak with varying d_1 in Fig. 2(c) is more obvious than that in Fig. 2(a), which indicates the coupling is more sensitive with higher analyte RI.

In order to understand the coupling properties further, we present the dispersion and loss of both core guided mode and plasmonic modes for higher analyte RI in Fig. 3. From the Fig. 3(a), we find that anti-crossing point occurs between the second-order plasmonic mode (black) and the core-guided mode, then the modes of each other exchanged after the anti-crossing point. In the case of $d_1 = 1.2\Lambda_2$ and $n_a = 1.392$, the complete coupling occurs as the
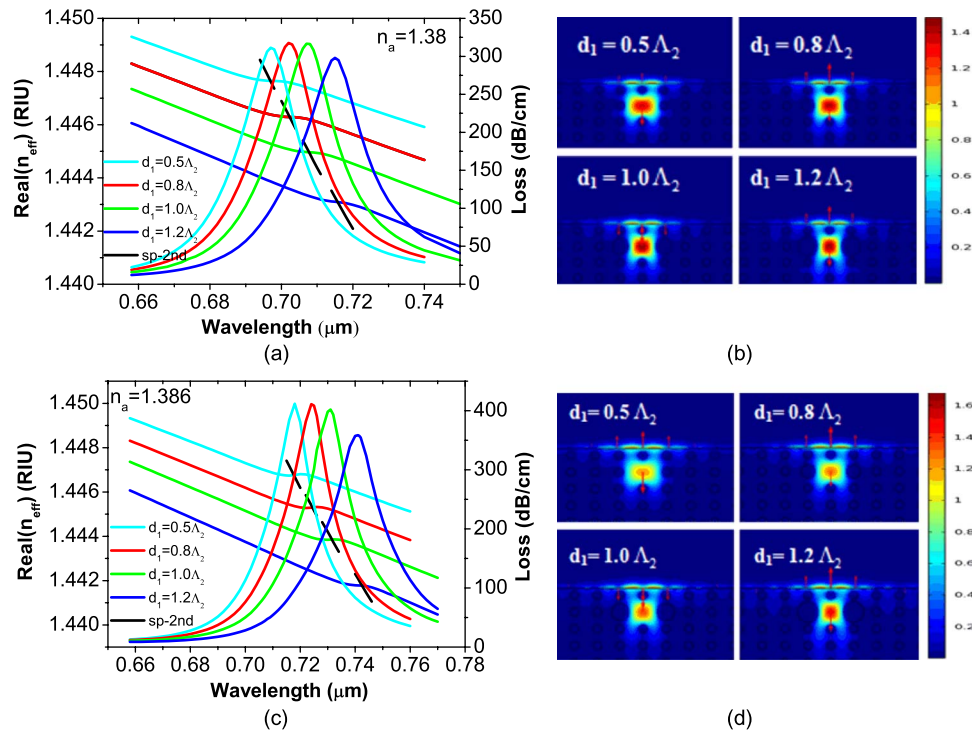
Fig. 2. (a), (c) Phase match condition and (b), (d) distribution of electric field near the resonance wavelength for four different diameters of $d_1 = 0.5\Lambda_2$, $0.8\Lambda_2$, $1.0\Lambda_2$, and $1.2\Lambda_2$ under the different analyte RI $n_a = 1.38$ and 1.386, respectively.

phase matching and loss matching condition are met simultaneously [3]. As depicted in Fig. 3(b), under this condition, it exhibits very different comparing with Fig. 2(b) and (d). Here, the electric field intensity of core guided mode with $d_1 = 1.2\Lambda_2$ is lowest, which is resulted in the complete coupling. The loss in the circumstance of complete coupling would get its apex through all values of analyte RI. The loss curves exhibit unsmooth at the region where wavelength shorter than resonant wavelength, this is because of the resonance occurring between higher order plasmonic mode and core mode. In Fig. 3, the coupling of second order plasmonic mode and core mode plays the major role, however, the resonance occurred between second order plasmonic mode and core mode becomes stronger with increasing the diameter of d_1 for higher RI. As the electric field direction odd plasmonic mode do not participate the resonance.

It apparently indicates that the structure of $d_1 = 1.0\Lambda_2$ is just arriving the complete coupling condition for the analyte RI $n_a = 1.394$ in Fig. 3(c). For the case of $d_1 = 0.8\Lambda_2$, it is very close to complete coupling as the s-shaped kinks of core mode dispersive curve become pronounced and the loss curve of plasmonic mode and core mode are nearly equal at resonant wavelength, the plasmonic fundamental mode and second-order mode are involvement in the intense resonance with the core fundamental mode simultaneously. Fig. 3(d) enhances our conclusion that complete coupling leads to more energy leaking from core mode to plasmonic mode, nevertheless, the case with smaller d_1 has higher loss peak at complete coupling.

From Fig. 3(a) and (c), we can see that fundamental plasmonic mode also occupies a disregarded place. In particular at high analyte n_a the loss valley of fundamental plasmonic mode gets its value almost as same as that of second plasmonic mode for d_1 smaller than $1.2\Lambda_2$, thereby, the wavelength difference of the loss valley of the two plasmonic modes would have a considerable influence on the whole coupling properties. If the difference is little enough then the resonance could be enhanced without changing the FWHM of the loss line of core guided mode.
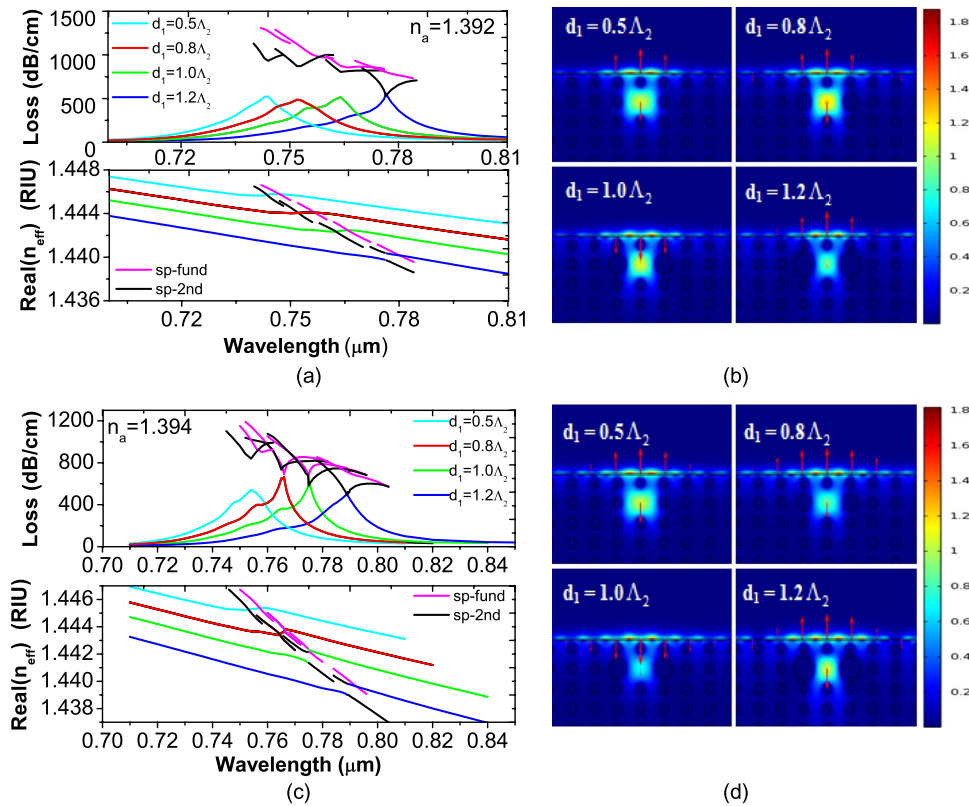
Fig. 3. (Left) Dispersive relationship and corresponding loss spectrum, and the confinement loss exhibits a peak at the crossing point or the anti-crossing point of the core mode and the plasmonic mode. (Right) Electric field distribution and electric orientation of fiber core for four diameter of d_1 under the analyte RI $n_a = 1.392$ and 1.394.
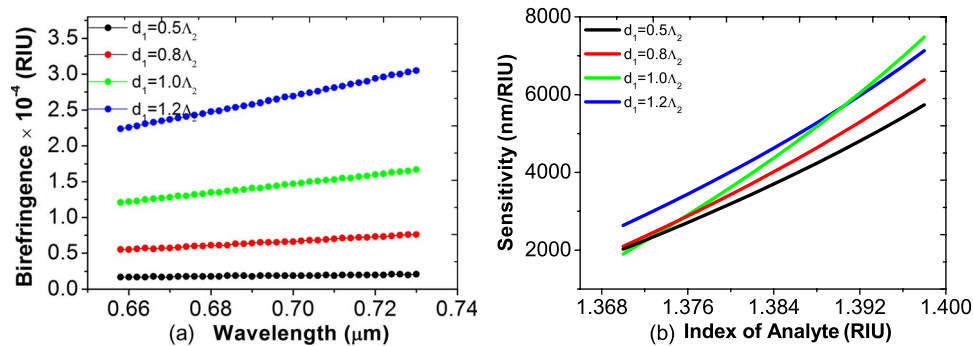

Fig. 4. (a) Birefringence through changing the diameter of d_1 with increasing of wavelength and (b) sensitivity of different hole sizes of d_1 with the increase of analyte RI. Different colors represent varying hole sizes of d_1.

3.2. The Influence of Hole Size on Sensor Performance

The variety of d_1 would obviously bring about the alteration of the birefringence, Fig. 4(a) presents different birefringence with different hole sizes of d_1. With the increasing of diameter of d_1, the birefringence increases. Moreover, the birefringence increases when the wavelength towards longer wavelength region, and for large air hole the birefringence increases sharply in the long wavelength. For the structure of $d_1 = 0.5\Lambda_2$ (0.75 μm), all air holes are equal, and in-herent birefringence of D-shaped structure is small and will not change with the wavelength
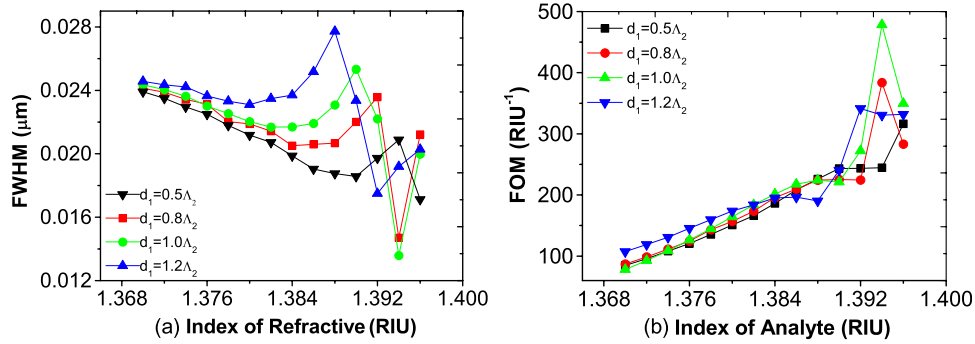
Fig. 5. (a) Deviation of FWHM for different diameter of d_1 with the increase of analyte RI. (b) FOM for different d_1 with the variation of analyte RI.

increasing in this circumstance [27]. As we have mentioned above, different hole sizes of d_1 will cause the change of the coupling properties consequently, as well as the sensitivity of the fiber. Fig. 4(b) gives the information of the sensitivity, it calculated by the differential of a fitting function. The magnitude of sensitivity arrange from up to down as d_1 is decreasing. It can be seen there is one irregular circumstance, that is sensitivity for $d_1 = 1.0\Lambda_2$. It is the least at the lowest analyte n_a, but it experiences a faster increase with increasing the analyte n_a than all others and finally exceeds them at the highest analyte n_a which the sensitivity can be up to 7481 nm/RIU. While the explicit reasons behind this keep unclear, the adjustment of the leaky channel arising from the variation of d_1 is obviously one of the reasons, another is that the resonance wavelengths of core mode interacts with second order plasmonic mode and fundamental order plasmonic mode, respectively, are nearly equal, as shown in Fig. 3, the superposition of the two resonances enhance the sensitivity. We also can reasonably consider that higher sensitivity exceeding 7481 nm/RIU will be achieve if $n_a > 1.398$ from the exponential function of Fig. 4(b), but the multi-peak loss spectrum which is not beneficial to the sensor will emerge under the analyte RI $n_a > 1.398$ [24], and low sensitivity is taken for the lower analyte RI $n_a < 1.37$. Thus, the appropriate dynamic detection range for n_a is from 1.37 to 1.398.

The full width at half maximum (FWHM) is an important parameter for sensor operation. And the detection's precise of resonance wavelength sharply depends on the width of the loss curve. A smaller FWHM is considerably effective to filter the spectral noise, resulting in lower spectral deviation from the actual center of the resonance wavelength and the suppression of the non-resonance confinement loss [28]. Fig. 5(a) displays FWHM for four different air hole sizes of d_1 with the analyte RI increases. Seeing that the peak appeared in the condition of low analyte RI for the larger hole size, and the dip of FWHM for $d_1 = 0.8\Lambda_2$, $1.0\Lambda_2$ both are the analyte RI $n_a = 1.394$. The lowest value of FWHM is 13.6 nm when the diameter of air hole is $d_1 = 1.0\Lambda_2$ under the $n_a = 1.394$.

Sensitivity provides a direct method to evaluate a sensor, however, the 'figure of merit' (FOM) is a more comprehensive parameter employing to measure the sensing performance and more widely accepted as defined in [29]

$$FOM = m(ev.RIU^{-1})/FWHM(ev) \qquad (2)$$

where m is the slope of the resonance peak position per RIU, it is better to indicate the sensitivity of the sensor as both of the absolute shift in energy and the width of the resonance peak have been put in the consideration. The discussed high FOM based MOFs sensing are 216 in reference [22] and 170 in reference [23], respectively. However, as was demonstrated in Fig. 5(b), our largest value of FOM obtained for $d_1 = 1.0\Lambda_2$ is 478.3 which is far exceeding the circumstances of other diameter of d_1 and previous reports. Higher FOM means better detective limit [30]. Therefore, we can realize that the structure of $d_1 = 1.0\Lambda_2$ has excellent performance in terms of sensor.
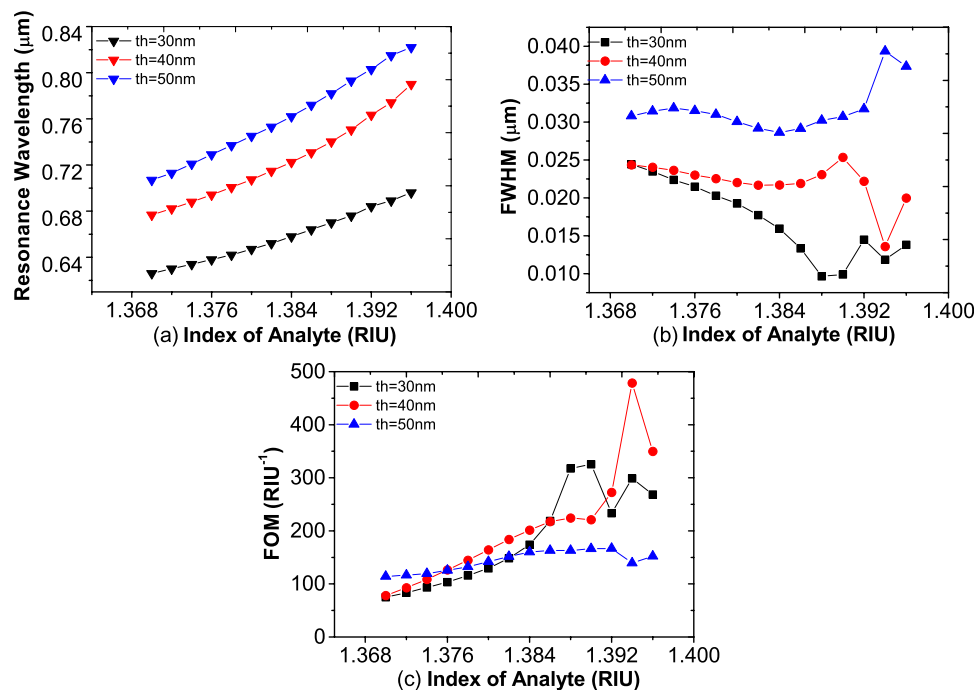
Fig. 6. Variations of (a) resonance wavelength, (b) FWHM, and (c) FOM for different thickness of gold film $th = 30$ nm (black), $th = 40$ nm (red), and $th = 50$ nm (blue) with the increasing of analyte RI.

3.3. Investigation of Varying the Thickness of the Gold Film

It is well known that the thickness of gold film has a sharp impact on the resonance coupling between the core-guided mode and plasmonic modes. In order to study the sensor performance further, we calculate (a) resonance wavelength, (b) FWHM, and (c) FOM for different thickness of gold film under the structure of $d_1 = 1.0\Lambda_2$ in Fig. 6. As shown in Fig. 6(a), the resonance wavelength moves to the longer wavelength region with the thickness of gold film increasing. FWHM in Fig. 6(b) represents the similar trend as Fig. 6(a), bigger thickness leads to larger FWHM. However, FOM achieves its highest value for the thickness of 40 nm during higher analyte RI, as a contrast, it keeps quite stable for thickness of 50 nm. That is because the strength of surface plasmon wave increases with the thickness of gold in a certain range. When the gold film is too thick, the electric field energy is not easy to penetrate through. And the variation of analyte refractive index will arouse the change of index difference then leading to the change of filed binding capacity. Therefore, there has an optimal thickness of gold film for different analyte RI range, the result agrees with the reference [30], [31]. Based on FOM calculated in different thickness of gold in the case of $d_1 = 1.0\Lambda_2$, we can observe that the thickness of about $th = 40$ nm has the best sensing performance for relatively higher analyte RI and the thickness of gold about 30 nm is also a right choice for relatively lower analyte RI.

4. Conclusion

We have discussed a D-shaped microstructured optical fiber deposited with gold film. By changing the size of air holes we chosen, birefringence has been introduced. The dispersion and loss spectral for different d_1 indicate that the complete coupling occurs at lower analyte RI for larger d_1. For all cases in uncompleted or complete coupling condition, large d_1 results in less loss of core mode, but the change of sensing performance is not linear with the alteration of d_1. High sensitivity and narrow FWHM are demonstrated in the circumstance of $d_1 = 1.0\Lambda_2$, and the best sensor performance evaluating via FOM is also exhibited in the case of $d_1 = 1.0\Lambda_2$. As the

thickness of the gold film is so important as well, we calculated its influence on the sensing performance to optimize the structure parameters further. Therefore, we assumed that our structure of diameter $d_1 = 1.0\Lambda_2$ has excellent sensing performance, which has the potential to be a competitive candidate in the application of sensor.

Acknowledgment

References

[1] J. Homola, *Surface Plasmon Resonance Based Sensors*. Berlin, Germany: Springer-Verlag, 2006.
[2] J. Zhou *et al.,* "Intensity modulated refractive index sensor based on optical fiber Michelson interferometer," *Sens. Actuators B, Chem.*, vol. 208, pp. 315–319, Nov. 2014.
[3] Z. H. Zhang, Y. F. Shi, B. M. Bian, and J. Lu, "Dependence of leaky mode coupling on loss in photonic crystal fiber with hybrid cladding," *Opt. Exp.*, vol. 16, no. 3, pp. 1915–1922, Feb. 2008.
[4] X. H. Zhao *et al.,* "Improvement of the sensitivity of the surface plasmon resonance sensors based on multi-layer modulation techniques," *Opt. Commun.*, vol. 335, pp. 32–36, Jan. 2015.
[5] Y. K. Gao *et al.,* "Plasmonic interferometric sensor arrays for high-performance label-free biomolecular detection," *Lab Chip*, vol. 13, no. 24, pp. 4755–4764, 2013.
[6] N. Livnat Levanon, E. Vigonsky, and O. Lewinson, "Real time measurements of membrane protein: Receptor interactions using Surface Plasmon Resonance (SPR)," *J. Vis. Exp.*, vol. 29, no. 93, p. e51937, Nov. 2014.
[7] J. N. Dash and Jha, "SPR biosensor based on polymer PCF coated with conducting metal oxide," *Photon. Technol. Lett.*, vol. 26, no. 6, pp. 595–598, Mar. 2014.
[8] A. Dhawan, M. D. Gerhold, and J. F. Muth, "Plasmonic structures based on subwavelength apertures for chemical and biological sensing applications," *IEEE Sens. J.*, vol. 8, no. 6, pp. 942–950, Jun. 2008.
[9] S. Zuccon, P. Zuppella, A. J. Corso, F. Gerlin, and M. G. Pelizzo, "Plasmonic response of different metals for specific applications," in *Proc. SPIE*, 2014, pp. 1–6.
[10] H. K. Tyagi, M. A. Schmidt, L. N. Prill Sempere, and P. St. John Russell, "Optical properties of photonic crystal fiber with integral micron-sized Ge wire," *Opt. Exp.*, vol. 16, no. 22, pp. 17227–17236, 2008.
[11] D. Noordegraaf *et al.,* "Avoid-crossing-based liquid-crystal photonic-bandgap notch filter," *Opt. Lett.*, vol. 33, no. 9, pp. 986–988, 2008.
[12] X. Zhang, R. Wang, F. M. Cox, B. T. Kuhlmey, and M. C. J. Large, "Selective coating of holes in microstructured optical fiber and its application to in-fiber absorptive polarizers," *Opt. Exp.*, vol. 15, no. 24, pp. 16270–16278, 2007.
[13] M. Schmidt, L. Prill Sempere, H. Tyagi, C. Poulton, and P. Russell, "Waveguiding and plasmon resonances in two-dimensional photonic lattices of gold and silver nanowires," *Phys. Rev. B*, vol. 77, no. 3, 2008, Art. ID. 033417.
[14] H. Kim, J. Kim, U.-C. Paek, B. H. Lee, and K. T. Kim, "Tunable photonic crystal fiber coupler based on a side-polishing technique," *Opt. Lett.*, vol. 29, no. 11, pp. 1194–1196, Jun. 2004.
[15] H. Y. Lin, Y. C. Tsai, Y. C. Tsao, and B. C. Sheu, "Side-polished multimode fiber biosensor based on surface plasmon resonance with halogen light," *Appl. Opt.*, vol. 46, no. 5, pp. 800–806, 2007.
[16] G. W. An *et al.,* "High-sensitivity refractive index sensor based on D-shaped photonic crystal fiber with rectangular lattice and nanoscale gold film," *Plasmonics*, vol. 9, no. 6, pp. 1355–1360, Dec. 2014.
[17] B. B. Zeng, Y. K. Gao, and F. J. Bartoil, "Rapid and highly sensitive detection using Fano resonances in ultrathin plasmonic nanogratings," *Appl. Phys. Lett.*, vol. 105, 2014, Art. ID. 161106.
[18] A. Barik *et al.,* "Dielectrophoresis-enhanced plasmonic sensing with gold nanohole arrays," *Nano Lett.*, vol. 14, no. 4, pp. 2006–2012, 2014.
[19] B. B. Zeng, Y. K. Gao, and F. J. Bartoli, "Differentiating surface and bulk interactions in nanoplasmonic interferometric sensor arrays," *Nanoscale*, vol. 7, pp. 166–170, 2015.
[20] A. A. Yanik *et al.,* "Seeing protein monolayers with naked eye through plasmonic Fano resonances," *Proc. Nat. Acad. Sci. USA*, vol. 108, no. 29, pp. 11784–11789, Feb. 2011.
[21] Y. Shen *et al.,* "Plasmonic gold mushroom arrays with refractive index sensing figures of merit approaching the theoretical limit," *Nature Commun.*, vol. 4, 2013, Art. ID. 2381.
[22] M. Tian, P. Lu, L. Chen, L. V. Chao, and D. M. Liu, "All-solid D-shaped photonic fiber sensor based on surface plasmon resonance," *Opt. Commun.*, vol. 285, pp. 1550–1554, 2012.
[23] Z. K. Fan *et al.,* "High sensitivity of refractive index sensor based on analyte-filled photonic crystal fiber with surface plasmon resonance," *IEEE Photon. J.*, vol. 7, no. 3, Jun. 2015, Art. ID. 4800809.
[24] F. K. Shi *et al.,* "An elliptical core D-shaped photonic crystal fiber-based plasmonic sensor at upper detection limit," *Plasmonics*, vol. 5, pp. 1–6, Mar. 2015.
[25] D. Rioux, S. Vallieres, S. Besner, E. Mazur, and M. Meunier, "An analytic model for the dielectric function of Au, Ag, and their alloys," *Adv. Opt. Mater.*, vol. 2, no. 2, pp. 176–182, Feb. 2014.
[26] W. Sellmeier, "Zur erklarung derabnormen farbenfolge im spectrum einiger substanzen," *Annalen Phys. Chem.*, vol. 219, no. 6, pp. 272–282, Feb. 1871.
[27] X. Yu *et al.,* "An efficient approach for investigating surface Plasmon resonance in asymmetric optical fibers based on birefringence analysis," *Opt. Exp.*, vol. 18, no. 17, pp. 17950–17957, 2010.

[28] B. B. Shuai, L. Xia, Y. T. Zhang, and D. M. Liu, "A multi-core holey fiber based plasmonic sensor with large detec-
tion range and high linearity," *Opt. Exp.*, vol. 20, no. 6, pp. 5974–5986, Mar. 2012.

[29] L. J. Sherry, S. H. Chang, G. C. Schatz, and D. R. P. Van, "Localized surface plasmon resonance spectroscopy of
single silver nanocubes," *Nano Lett.*, vol. 5, no. 10, pp. 2034–2038, 2005.

[30] X. Yu *et al.,* "A selectively coated photonic crystal fiber based surface plasmon resonance sensor," *J. Opt.*, vol. 12,
no. 1, pp. 1–4, Jan., 2010.

[31] J. R. Xue *et al.,* "Polarization filter characters of the gold-coated and the liquid filled photonic crystal fiber based on
surface plasmon resonance," *Opt. Exp.*, vol. 21, no. 11, pp. 13 733–13 740, 2013.